ALZHEIMER'S DISEASE

10.1126/sciadv.1500472

Autoregulated paracellular clearance of amyloid-β across the blood-brain barrier

James Keaney,[1] Dominic M. Walsh,[2] Tiernan O'Malley,[2] Natalie Hudson,[1] Darragh E. Crosbie,[1] Teresa Loftus,[3] Florike Sheehan,[3] Jacqueline McDaid,[1] Marian M. Humphries,[1] John J. Callanan,[4,5] Francesca M. Brett,[3] Michael A. Farrell,[3] Peter Humphries,[1] Matthew Campbell[1]*

The blood-brain barrier (BBB) is essential for maintaining brain homeostasis and protecting neural tissue from damaging blood-borne agents. The barrier is characterized by endothelial tight junctions that limit passive paracellular diffusion of polar solutes and macromolecules from blood to brain. Decreased brain clearance of the neurotoxic amyloid-β (Aβ) peptide is a central event in the pathogenesis of Alzheimer's disease (AD). Whereas transport of Aβ across the BBB can occur via transcellular endothelial receptors, the paracellular movement of Aβ has not been described. We show that soluble human Aβ(1–40) monomers can diffuse across the paracellular pathway of the BBB in tandem with a decrease in the tight junction proteins claudin-5 and occludin in the cerebral vascular endothelium. In a murine model of AD (Tg2576), plasma Aβ(1–40) levels were significantly increased, brain Aβ(1–40) levels were decreased, and cognitive function was enhanced when both claudin-5 and occludin were suppressed. Furthermore, Aβ can cause a transient down-regulation of claudin-5 and occludin, allowing for its own paracellular clearance across the BBB. Our results show, for the first time, the involvement of the paracellular pathway in autoregulated Aβ movement across the BBB and identify both claudin-5 and occludin as potential therapeutic targets for AD. These findings also indicate that controlled modulation of tight junction components at the BBB can enhance the clearance of Aβ from the brain.

INTRODUCTION

Alzheimer's disease (AD) is a progressive neurodegenerative disorder characterized by a gradual decline in cognitive function and is the most common cause of dementia in the elderly. Currently, there are about 36 million people worldwide who suffer from AD and other dementias, and there are no approved medicines to prevent disease progression (*1*). The central neuropathologic hallmarks of AD are (i) the extracellular accumulation of the amyloid-β protein (Aβ) in parenchymal plaques (*2*) and (ii) the formation of intracellular neurofibrillary tangles composed of hyperphosphorylated forms of the microtubule associated protein tau (*3*). More recently, impaired clearance of pathogenic soluble Aβ species from the brain has been identified as a major factor in AD pathogenesis (*4*–*6*). This leads to the accumulation of Aβ around cerebral blood vessels, a condition known as cerebral amyloid angiopathy (CAA), which is found in more than 80% of AD patients (*7*). Aβ deposition in the cerebral vasculature causes significant damage to central nervous system (CNS) endothelial cells, contributing to a range of characteristic CAA-associated neurovascular anomalies including lobar hemorrhage, cerebral microbleeds, ischemic stroke, and chronic vascular inflammation (*7*).

CNS endothelial cells along with astrocytes and pericytes constitute the blood-brain barrier (BBB), a complex and dynamic system that acts as a biological interface between blood and brain (*8*, *9*). As well as regulating the exchange of ions and macromolecules between the blood and the neural microenvironment, cerebrovascular endothelial cells (CVECs) protect the brain by restricting the entry of potentially damaging blood-borne agents such as neurotoxic chemicals, antibodies, pathogens, immune cells, and anaphylatoxins. As such, the BBB plays a pivotal role in maintaining CNS homeostasis, and CVECs have evolved properties distinct from peripheral endothelial cells (*10*). CVECs are linked by tight junction protein complexes, which limit paracellular transport between adjacent cells. Furthermore, the transcellular movement of nutrients into the brain and the efflux of metabolites and toxins are controlled by a number of specific transporter proteins (*11*). In the context of Aβ transport at the BBB, low-density lipoprotein receptor–related protein 1 (LRP1) has been implicated in active transcellular Aβ transport from brain to blood, whereas receptor for advanced glycation end products (RAGE) has been suggested to facilitate the movement of Aβ from blood to brain (*12*, *13*). Aβ has been shown to induce alterations in tight junction protein expression in vitro and in vivo (*14*–*16*), yet the role of the tight junction and distinct tight junction components in the molecular etiology and pathophysiology of AD is not well defined.

Here, we show that targeted knockdown of the tight junction proteins, claudin-5 and occludin, using RNA interference (RNAi), facilitates the diffusion of Aβ(1–40) monomers across brain endothelial cells in vitro and size-selectively modulates BBB permeability in vivo. In the Tg2576 mouse model of AD, cosuppression of claudin-5 and occludin enhanced the efflux of Aβ monomers from the brain to the blood and ameliorated Aβ-associated cognitive deficits. Furthermore, small soluble Aβ species were found to transiently down-regulate both claudin-5 and occludin at the posttranslational level, suggesting that Aβ itself could modulate tight junction complexes. Finally, reduced claudin-5 and occludin levels were recorded in both aged Tg2576 mouse brains and human AD brains, specifically in response to Aβ along CAA-affected vessels. These data indicate that soluble Aβ can function in a transient

[1]Smurfit Institute of Genetics, Lincoln Place Gate, Trinity College Dublin, Dublin 2, Ireland. [2]Laboratory for Neurodegenerative Research, Center for Neurological Diseases, Brigham and Women's Hospital, Harvard Institute of Medicine, 77 Avenue Louis Pasteur, Boston, MA 02115, USA. [3]Department of Neuropathology, Beaumont Hospital, Dublin 9, Ireland. [4]UCD School of Veterinary Medicine and Conway Institute of Biomolecular and Biomedical Research, University College Dublin, Belfield, Dublin 4, Ireland. [5]Ross University School of Veterinary Medicine, P. O. Box 334, Basseterre, St. Kitts, West Indies.
*Corresponding author. E-mail: matthew.campbell@tcd.ie

and autoregulated manner to allow for its own paracellular clearance across the BBB, and that therapeutic strategies aimed at targeting claudin-5 and occludin at the BBB may provide a novel means to treat AD. In addition, our findings add considerable weight to the "amyloid sink hypothesis" that has been associated with recent clinical trials using anti-Aβ antibodies.

RESULTS

Soluble Aβ size-selectively diffuses across the paracellular pathway of cerebral microvascular endothelial cells in vitro

Whereas transcellular receptors in brain endothelial cells have been implicated in Aβ entry and clearance across the BBB, the potential for Aβ movement along paracellular routes has not been explored in detail. Using small interfering RNAs (siRNAs) designed to target claudin-5 and occludin, two major tight junction components sealing the paracellular gap, we assessed the movement of small soluble Aβ species across monolayers of mouse brain endothelial cells (Bend.3 cell line). First, we found that siRNAs directed against the transcripts of each protein caused potent target suppression in brain endothelial cells (Fig. 1, A and B) without affecting the levels of the intracellular ZO-1 protein (fig. S1), and this was accompanied by a significant decrease in transendothelial electrical resistance (TEER) (Fig. 1C). Next, we examined the effect of claudin-5 and occludin knockdown on the paracellular diffusion of fluorescein isothiocyanate (FITC)–labeled Aβ(1–40) across intact brain endothelial cell monolayers (Fig. 1D). The addition of fluorescently labeled Aβ(1–40) to the apical aspect of cells showed that this molecule was able to move across the paracellular pathway, and its rate of diffusion was enhanced when both claudin-5 and occludin were suppressed (Fig. 1D). In addition, when FITC–Aβ(1–40) was added to the basolateral aspect of cells, it diffused along its own concentration gradient, and this was enhanced when both claudin-5 and occludin were suppressed (Fig. 1E). Similarly, enhanced diffusion of Aβ(1–42) (fig. S2) and a metabolically inert polar molecule, inulin (fig. S3), both conjugated to FITC, was observed when claudin-5 and occludin levels were modulated. Furthermore, isolation and transfection of primary mouse brain endothelial cells with claudin-5 and/or occludin siRNAs decreased TEER and enhanced the basolateral-to-apical movement of FITC–Aβ(1–40) (fig. S4). This increase in FITC–Aβ(1–40) diffusion after tight junction protein suppression was retained after the silencing of the transcellular Aβ receptor LRP1 (fig. S4).

Because wild-type Aβ can readily self-associate to form oligomers and aggregates, we next applied a design Aβ monomer, in which Phe at position 19 is replaced by Pro (F19P) and which shows little or no propensity for aggregation (*17*). Furthermore, to assess potential size selectivity after claudin-5 and occludin down-regulation, we also used a dityrosine cross-linked dimer [Aβ(1–40)DiY] (*18*). Intriguingly, whereas the Aβ(1–40)F19P monomer diffused across the paracellular pathway of endothelial cells in a process regulated by the levels of claudin-5 and occludin, the Aβ(1–40)DiY dimer did not diffuse to the same extent (Fig. 1F). These results indicate the presence of a size-selective tight junction in vitro that was permeable to molecules of about 4.3 kD but not 8.7 kD when claudin-5 and occludin levels were simultaneously decreased. In addition, diffusion of Aβ(1–40)F19P across brain microvascular endothelial cell monolayers was even enhanced when physiological nanomolar amounts of the monomer peptide were used (see fig. S5).

RNAi-mediated suppression of claudin-5 and occludin size-selectively modulates the BBB in vivo

Because simultaneous down-regulation of claudin-5 and occludin could enhance the flux of Aβ monomers but not dimers across brain endothelial cells in vitro, this size selectivity led us to examine the effects of claudin-5 and occludin cosuppression on BBB permeability in vivo. We began by intravenously injecting siRNAs directed against claudin-5 and occludin transcripts in wild-type mice. Given the differing half-lives of claudin-5 (about 30 hours) and occludin proteins (about 60 hours), the siRNA injections were staggered by 24 hours to allow for simultaneous cosuppression of transcripts and proteins in brain capillary enriched fractions (fig. S6). Indeed, cosuppression of claudin-5 and occludin resulted in a decreased concentration of these tight junction components in the microvasculature of the brain (Fig. 2, A to C) and caused an increased extravasation of the magnetic resonance imaging (MRI) contrast agent gadolinium–diethylenetriamine pentaacetic acid (Gd-DTPA; about 800 daltons) (Fig. 2D).

Whereas we have previously shown that in vivo suppression of claudin-5 transcripts at the BBB in mice causes a size-selective increase in BBB permeability to molecules below about 1 kD (*19*), we wanted to ascertain whether cosuppression of claudin-5 and occludin could further increase this size selectivity in a manner similar to that already observed in vitro. After perfusion of mice with a biotinylated dextran (3 kD MW), we observed increased extravasation at the BBB when claudin-5 and occludin were cosuppressed (Fig. 2E, top). However, perfusion of a biotinylated dextran of 10 kD MW did not show any signs of extravasation (Fig. 2E, bottom), indicating a role for claudin-5 and occludin in mediating size-selective diffusion across the paracellular pathway of the BBB. Enhanced extravasation of 3-kD biotin-dextran was also observed after administration of claudin-5 and occludin siRNAs in the amyloid precursor protein/presenilin 1 (APP/PS1) mouse model of AD (fig. S7). In addition, cosuppression of these two tight junction components did not seem to have a deleterious effect on any peripheral organs after perfusion with biotin-dextran (fig. S8).

Down-regulation of claudin-5 and occludin enhances paracellular clearance of Aβ from the brains of Tg2576 mice and improves cognitive function

Because we observed an increase in Aβ flux when claudin-5 and occludin were cosuppressed in vitro and a size-selective increase in BBB permeability after claudin-5 and occludin suppression in wild-type mice, we were stimulated to assess the effects of tight junction protein modulation on Aβ transport in a murine model of AD, namely, the Tg2576 mouse that overexpresses a double mutant form of human APP leading to increased brain Aβ levels and impaired cognitive function. Having shown that intravenous injection of claudin-5 and occludin siRNAs allowed for tight junction protein suppression in vessels of Tg2576 mouse brains (Fig. 3A), we chronically administered (once every 21 days for a period of 9 months) young Tg2576 mice with siRNAs targeting occludin and claudin-5 and collected blood at 72 to 96 hours after injection. A sustained increase in Aβ(1–40) was observed in plasma samples isolated from claudin-5 and occludin (C/O) siRNA–treated compared to nontargeting (NT) siRNA–treated animals (Fig. 3B). Whereas plasma levels of Aβ(1–40) were somewhat lower than has been previously reported (*20*), we ensured that all samples were simultaneously analyzed on the same enzyme-linked immunosorbent assay (ELISA) plates. To examine the effects of increased brain-to-blood Aβ movement on cognitive function in these animals, we used the T-maze

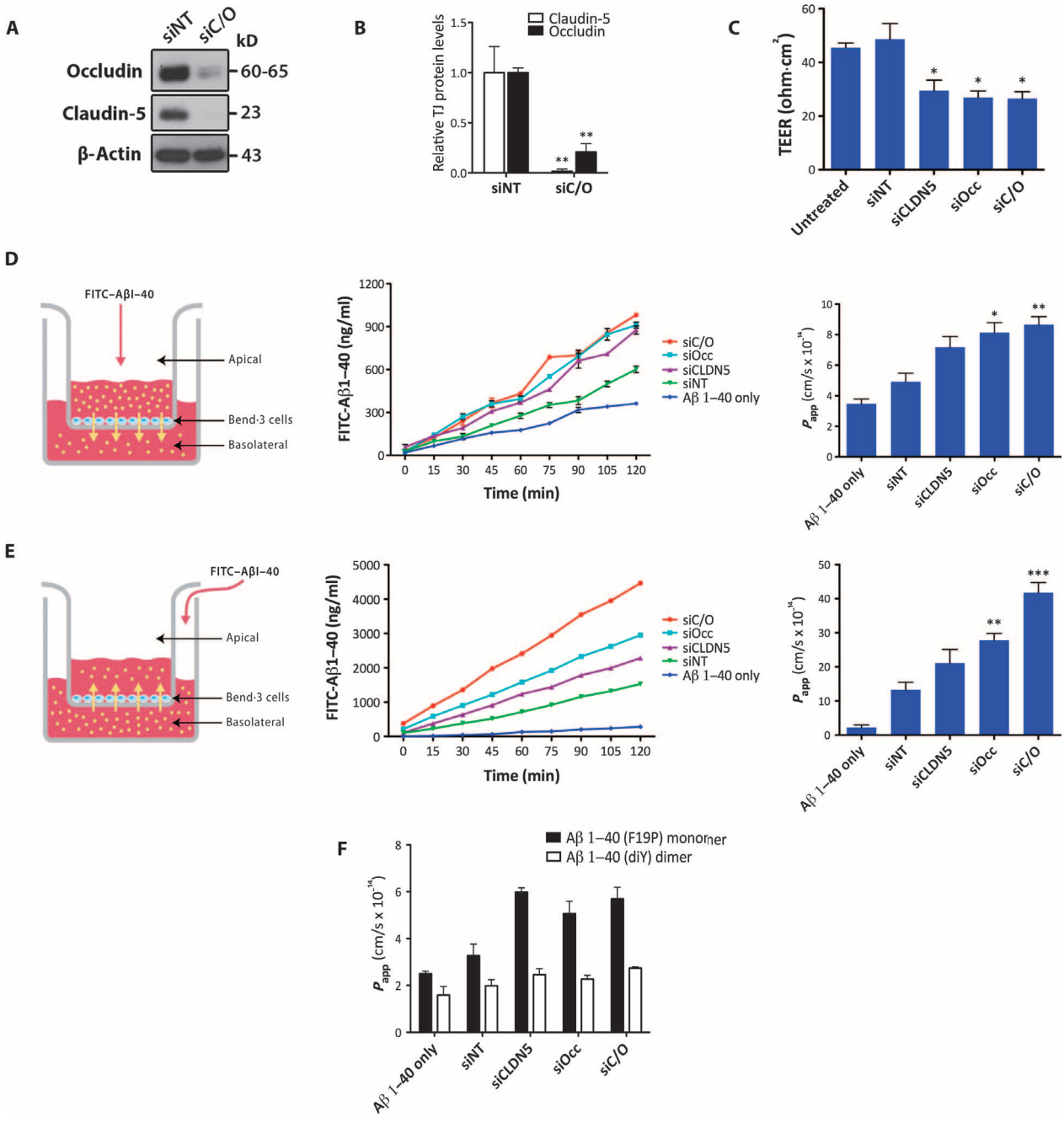

Fig. 1. Down-regulation of claudin-5 and occludin (C/O) in mouse brain endothelial cells allows size-selective movement of Aβ(1–40) peptides across cell monolayers. (**A**) Western blot of claudin-5 and occludin protein levels 72 hours after siRNA transfection (C/O, claudin-5 and occludin siRNAs). (**B**) Densitometric analysis of relative protein levels normalized to a NT siRNA sample at each time point (unpaired Student's *t* test: $^{**}P \leq 0.01$; data are means ± SEM, $n = 3$ separate cell transfections). (**C**) TEER measurements across brain endothelial cell monolayers after treatment with NT siRNA, claudin-5 siRNA, occludin siRNA, or C/O siRNAs [one-way analysis of variance (ANOVA) followed by Bonferroni's post hoc test for multiple comparisons: $^{*}P \leq 0.05$ compared to siNT treatment; 95% confidence interval; data are means ± SEM, $n = 3$ separate cell transfections]. (**D**) Schematic diagram of FITC–Aβ(1–40) application to the apical chamber of a Transwell plate and its movement across brain endothelial cell monolayers (left). FITC–Aβ(1–40) peptide was applied to the apical chamber of a Transwell plate 72 hours after siRNA treatment of brain endothelial cells, and its movement across cell monolayers was monitored by fluorescence spectrophotometry over the course of 2 hours (middle). The apparent permeability coefficient (P_{app}) was also measured for all siRNA treatments (one-way ANOVA followed by Bonferroni's post hoc test for multiple comparisons: $^{*}P \leq 0.05$, $^{**}P \leq 0.01$, $^{***}P \leq 0.001$, all compared to siNT treatment; 95% confidence interval; data are means ± SEM, $n = 3$ separate cell transfections) (right). (**E**) Schematic diagram of FITC–Aβ(1–40) application to the basolateral chamber (left), movement of FITC–Aβ(1–40) from the basolateral to the apical chamber (middle), and P_{app} for movement of FITC–Aβ(1–40) from the basolateral to the apical chamber (right). (**F**) Comparison of apparent permeability coefficients (P_{app}) for synthetic Aβ(1–40)F19P monomer and Aβ(1–40)DiY dimer after apical application and movement across brain endothelial cell monolayers.

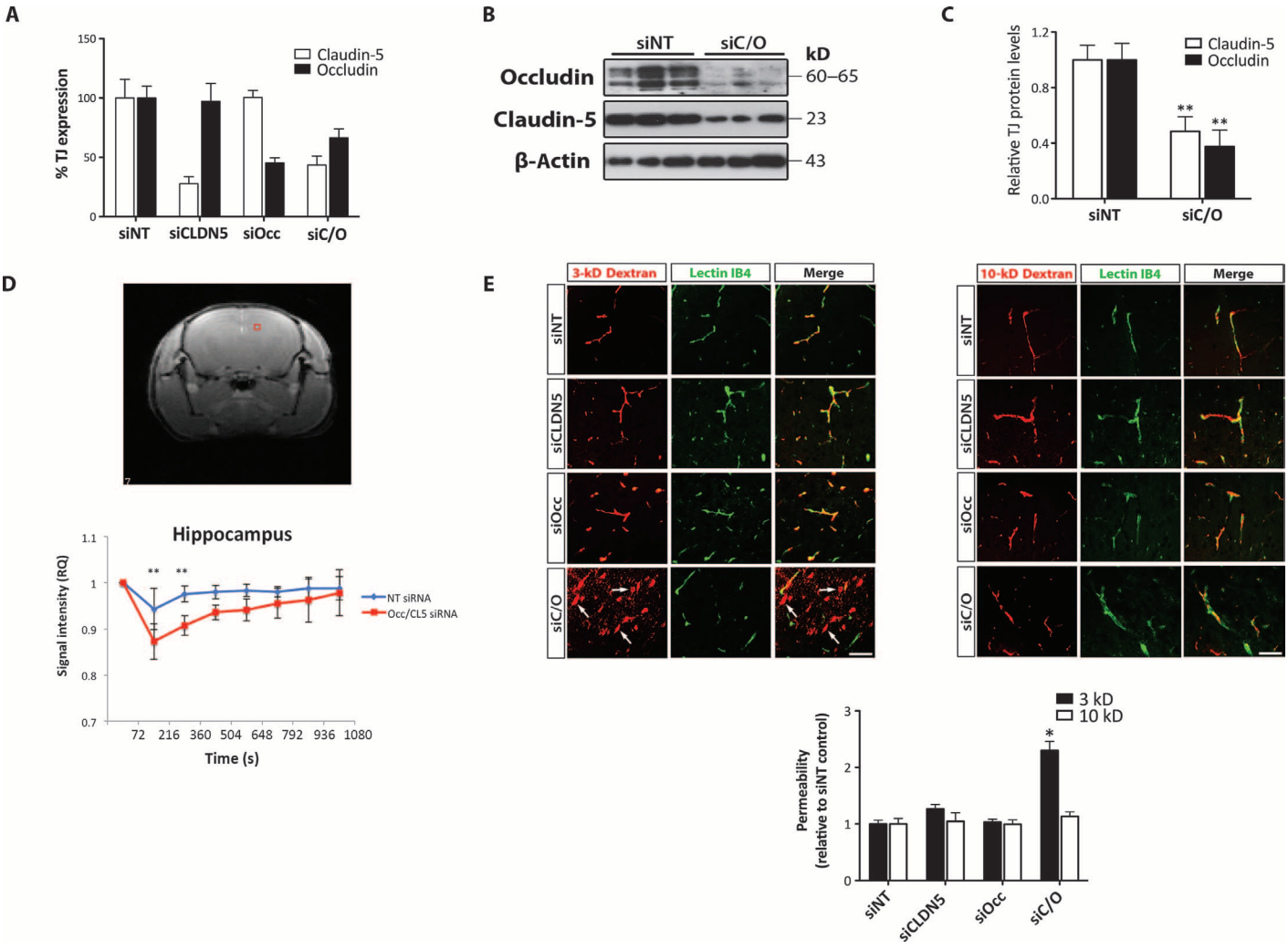

Fig. 2. In vivo cosuppression of claudin-5 and occludin and assessment of BBB permeability in claudin-5 and occludin (C/O) siRNA–treated mice. (**A**) Transcript levels of claudin-5 and occludin as measured by RT-PCR in brain capillary fractions isolated from animals treated with nontargeting (NT) siRNA or C/O siRNAs ($n = 3$ to 4 animals per treatment; data are means ± SEM). (**B**) Western blot of claudin-5 and occludin protein levels in brain capillary fractions isolated from NT siRNA– or C/O siRNA–treated animals. (**C**) Densitometric analysis of claudin-5 and occludin protein levels in brain capillary fractions isolated from NT siRNA– or C/O siRNA–treated animals (unpaired Student's t test: $^{**}P \leq 0.01$; data are means ± SEM, $n = 4$ to 5 animals per treatment). (**D**) Contrast-enhanced MRI and bolus chase analysis of clearance rates of Gd-DTPA (742 daltons) in hippocampal regions after tail-vein injection of the contrast agent in animals treated with NT siRNA or C/O siRNAs (unpaired Student's t test: $^{**}P \leq 0.01$; data are means ± SD, $n = 4$ animals per treatment). (**E**) Top: Animals treated with NT siRNA, claudin-5 siRNA, occludin siRNA, or C/O siRNAs were given a transcardial perfusion of 3-kD (left) or 10-kD (right) biotin-dextran, and brain sections were stained with isolectin IB4 and streptavidin-Cy3 (scale bars, 50 μm). Bottom: Streptavidin-Cy3 fluorescence measurements relative to NT siRNA control (one-way ANOVA followed by Bonferroni's post hoc test for multiple comparisons: $^{*}P < 0.05$, siC/O versus siNT; 95% confidence interval; data are means ± SEM, $n = 3$ to 4 animals per treatment).

test of hippocampal spatial memory (*21*). Mice receiving the combined claudin-5 and occludin siRNAs displayed significantly increased alternating behavior (mean, 68.51%) compared to NT siRNA–treated animals (mean, 62.54%) (Fig. 3C). At the end of this experiment and after perfusion of mice to clear systemic Aβ, we analyzed the levels of Aβ(1–40) in the brains. We observed a significant decrease in the levels of Aβ(1–40) in the brains of mice receiving the combined siRNAs compared to control animals (Fig. 3D). In a second AD mouse model, namely, double transgenic APP/PS1 mice, plasma Aβ(1–40) levels were elevated after claudin-5 and occludin cosuppression, with plaque number unchanged when compared to control animals (fig. S9). In addition, in the DBA/2J mouse strain where Aβ accumulates in the neural tissue of the retina with age (*22*), we observed a similar decrease in Aβ(1–40) levels in the retina after suppression of claudin-5 and occludin (fig. S10).

Because changes in the levels of the transcellular Aβ receptors, LRP1 and RAGE, can also alter Aβ transport across the BBB (*6*), we sought to assess whether claudin-5 and occludin cosuppression may indirectly affect LRP1/RAGE levels and account for increased plasma Aβ(1–40) levels. We found no significant differences in the expression pattern of these proteins in brain vascular fractions (Fig. 4A), in total brain fractions (Fig. 4B), or in liver fractions (the site of systemic Aβ clearance; Fig. 4C). Furthermore, the brain and liver levels of apolipoprotein E

(ApoE), which is involved in Aβ transport and clearance (*23*), and APP were unchanged between the siRNA treatment groups. These results suggest that enhanced Aβ(1–40) plasma levels in siRNA-treated Tg2576 mice are a direct result of claudin-5 and occludin suppression. In addition, these chronic injections of siRNA in mice did not induce changes in BBB permeability to large plasma proteins such as immunoglobulins (fig. S11). At the termination of this experiment, no histopathological evidence of toxicity was observed when the peripheral organs of these animals were examined (fig. S12).

Reduced claudin-5 and occludin in aged Tg2576 mouse brains in response to soluble Aβ

Given that aberrant tight junction protein expression has previously been described in clinical AD samples (*14*) and in AD mouse models (*15*, *16*), we next sought to evaluate the physiological integrity of the cerebral microvasculature because it pertained to the tight junctions in Aβ-rich environments. In this regard, measurements of TEER across confluent monolayers of primary brain endothelial cells isolated from aged (20 months) Tg2576 mice and age-matched wild-type controls showed significant decreases in TEER values across cell monolayers derived from aged Tg2576 mouse brains (Fig. 5A). This coincided with reduced levels of claudin-5 and occludin but no major changes in the other tight junction proteins, ZO-1 and tricellulin, as assessed by the Western blot (Fig. 5B). Whereas these in vitro analyses may constrain the interpretation of the in vivo BBB, immunohistochemical analysis of aged Tg2576 mouse brains showed that claudin-5 and occludin levels were specifically decreased along CAA-affected microvessels with intact claudin-5 and occludin immunostaining in areas with no Aβ deposition (Fig. 5C and fig. S13).

Because decreased claudin-5 and occludin along Aβ-laden vessels in aged Tg2576 mice is associated with increased BBB permeability and RNAi-mediated cosuppression of these proteins increases soluble Aβ flux across the BBB, we next sought to determine whether soluble Aβ alone can modulate tight junction protein levels. Using the soluble Aβ(1–40) monomer and dimer peptides used previously (*17*, *18*), we found that increasing doses of Aβ(1–40) monomers and dimers down-regulated the levels of claudin-5 and occludin, with the levels of the intracellular tight junction component ZO-1 remaining unchanged (Fig. 5D, top). Whereas the addition of Aβ(1–40) monomers and dimers caused a transient and reversible decrease in claudin-5 and occludin, there was

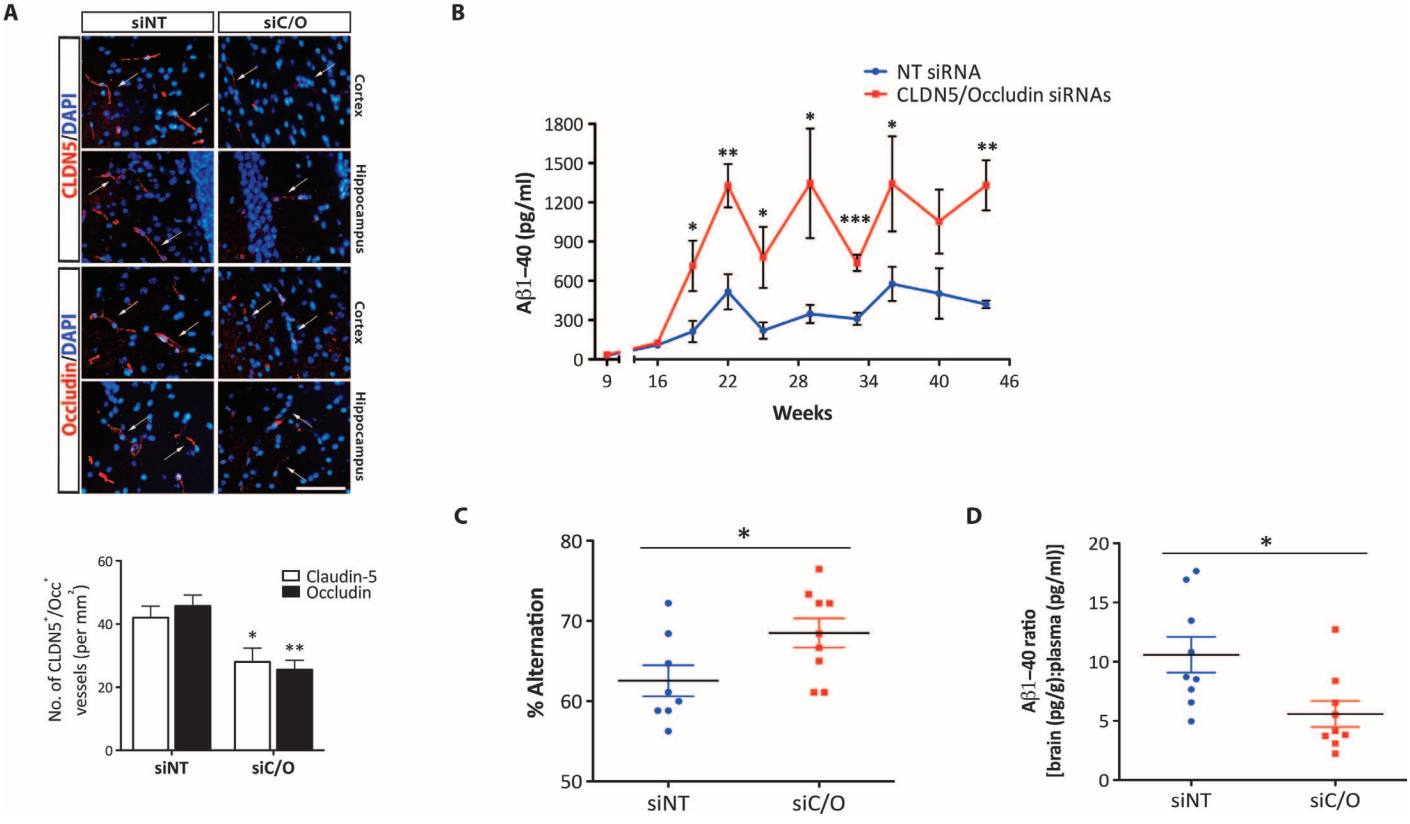

Fig. 3. Systemic administration of claudin-5 and occludin (C/O) siRNAs enhances the paracellular movement of amyloid-β (Aβ) 1–40 from brain to blood in Tg2576 transgenic mice. (**A**) Top: Immunohistochemical analysis of occludin and claudin-5 levels in brain microvessels after injection of siRNAs in Tg2576 mice (scale bar, 100 μm). Bottom: Quantification of claudin-5– and occludin-positive vessels in siRNA-treated Tg2576 mice (unpaired Student's *t* test: $^{*}P = 0.0406$ for claudin-5, $^{**}P = 0.0036$ for occludin; data are means ± SEM, $n = 4$ to 6 animals per experimental group). (**B**) ELISA of plasma Aβ(1–40) levels in Tg2576 mice after intravenous administration of nontargeting (NT) siRNA or C/O siRNAs (unpaired Student's *t* test: $^{*}P \leq 0.05$, $^{**}P \leq 0.01$, $^{***}P \leq 0.001$; data are means ± SEM, $n = 4$ to 6 animals per experimental group). (**C**) T-maze assessment of hippocampal-linked spatial memory as measured by percentage alternation rates in NT siRNA– or C/O siRNA–treated Tg2576 mice at 6 months of age (unpaired Student's *t* test: $^{*}P = 0.0403$; $n = 8$ to 9 animals per experimental group). (**D**) ELISA of brain/plasma Aβ(1–40) ratios [pg/g soluble brain Aβ(1–40) per pg/ml plasma Aβ(1–40)] in NT siRNA– or C/O siRNA–treated Tg2576 mice (unpaired Student's *t* test: $^{*}P = 0.0159$; $n = 9$ animals per group).

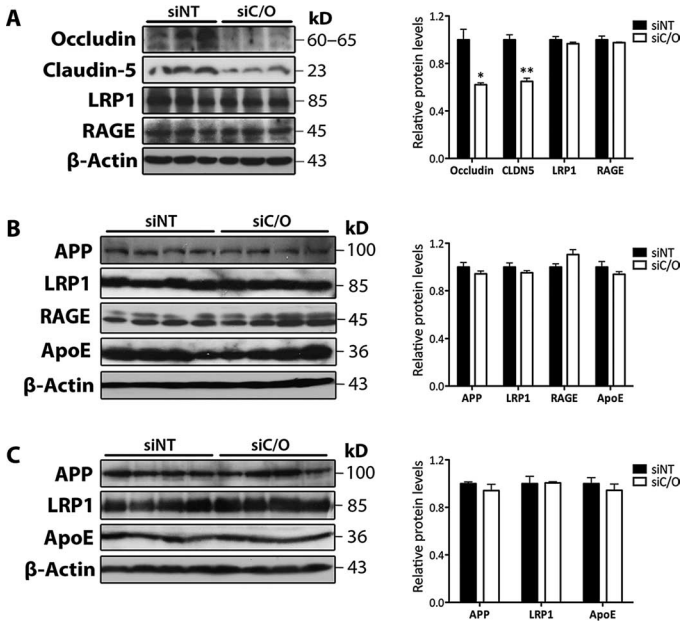

Fig. 4. RNAi-mediated cosuppression of claudin-5 and occludin (C/O) in Tg2576 mice does not affect the levels of major Aβ receptors and transporters. (**A**) Western blot (left) and densitometric analysis (right) of claudin-5, occludin, LRP1, and RAGE in brain vascular protein fractions isolated from NT siRNA– or C/O siRNA–treated Tg2576 mice (unpaired Student's *t* test: $*P \leq 0.05$, $**P \leq 0.01$; data are means ± SEM, $n = 3$ animals per treatment). (**B**) Western blot (left) and densitometric analysis (right) of APP, LRP1, RAGE, and ApoE in total brain protein fractions isolated from siRNA-treated Tg2576 mice (data are means ± SEM). (**C**) Western blot (left) and densitometric analysis (right) of APP, LRP1, RAGE, and ApoE in liver protein fractions isolated from siRNA-treated Tg2576 mice (data are means ± SEM).

an apparent rebound up-regulation of both occludin and ZO-1, 24 and 48 hours after treatment (Fig. 5D, bottom). Immunocytochemical analysis of claudin-5 and occludin localization showed a decrease in the punctate staining of both proteins 6 and 12 hours after treatment with Aβ(1–40) monomers and dimers (Fig. 5E). This was a transient response, with the protein levels returning to baseline 48 hours after treatment (Fig. 5E). The localization of ZO-1 at the tight junctions did not decrease at any time point after treatment, and similar to the Western blot analysis, there was an overt up-regulation in ZO-1 levels at the cell periphery (Fig. 5E). Size-exclusion isolated Aβ(1–40) monomers caused a similar dose-dependent decrease in claudin-5 and occludin levels (fig. S14).

Given the dynamic dose- and time-dependent effects that Aβ(1–40) monomers and dimers displayed on the levels of tight junction proteins, these results suggested that Aβ peptides might have an impact on transcriptional regulation of tight junction components. To our surprise, however, we did not observe any decreases in claudin-5 or occludin transcripts at any time point after treatment with Aβ(1–40) monomers or dimers (Fig. 5F). The levels of occludin transcript were up-regulated 24 to 48 hours after treatment with Aβ(1–40) monomers or dimers, whereas ZO-1 transcripts were significantly increased 6, 12, 24, and 48 hours after treatment, which is reflected by the increases seen at the protein level (Fig. 5F). Aβ did not alter the viability of brain endothelial cells, even at concentrations five times greater than that which caused changes in the levels and localization of occludin and claudin-5 (fig. S15). These results suggest that whereas transcriptional changes may account for tight junction protein up-regulation at later time points, loss of tight junction proteins after Aβ exposure is likely due to posttranslational modifications of claudin-5 and occludin that ultimately lead to their degradation.

Aβ accumulation and CAA segregates with reduced claudin-5 and occludin at the BBB in AD patients

To assess whether the spatial relationship between Aβ and the tight junction protein changes observed in Tg2576 mice and in mouse-brain endothelial cells pertains to human AD, we next determined the status of claudin-5 and occludin relative to the appearance of Aβ accumulation in postmortem human brains from a neurological disease cohort. Claudin-5 and occludin immunoreactivity was observable throughout the brain sections analyzed from nonneurodegenerative cases such as traumatic brain injury (contralateral to site of injury) and non-AD neurodegenerative cases such as progressive supranuclear palsy, amyotrophic lateral sclerosis, and Lewy body dementia (Fig. 6, A and B). However, the presence of Aβ/CAA in AD cases seemed to correlate strongly with a decrease in the vascular levels of claudin-5 and occludin (Fig. 6, A and B). Moreover, in AD donor brains, intact claudin-5 and occludin staining was evident in CAA-free blood vessels proximal to Aβ plaques (Fig. 6C).

DISCUSSION

The role of Aβ in AD pathogenesis was first established after the discovery that AD could be inherited in an autosomal dominant fashion as a result of a mutation in the gene coding for APP (*24*). However, after the recent setbacks associated with clinical trials of Aβ-targeting antibodies, it has become clear that a greater understanding of the early disease process will be key to therapeutic strategies aimed at preventing or at least ameliorating AD. There is now a broad consensus that AD starts many years before memory problems become apparent, and that treatment may be too late when patients already have dementia (*25*). Recent data strongly suggest that aberrant clearance of Aβ is likely to play a significant, if not central, role in late-onset AD (*5*). To date, much attention has focused on understanding the transcellular movement of Aβ via LRP1 and RAGE receptors (*6*, *12*, *13*), but surprisingly, little is known about the paracellular movement of Aβ in normal, presymptomatic, or indeed AD-affected individuals. Tight junction "dysfunction" has been previously associated with the molecular pathology of AD (*14*–*16*); however, the underlying role and consequences of these tight junction changes have never been elucidated. Because claudin-5 and occludin are major regulators of paracellular permeability between endothelial cells of the brain vasculature (*26*–*28*), decreased levels of claudin-5 and occludin in CAA vessels of human AD and murine Tg2576 brains in response to Aβ(1–40) monomers and dimers also indicated a potential involvement of Aβ transport across the BBB. Indeed, it was apparent that both forms of Aβ(1–40) could elicit transient modulation of the tight junction; however, using in vivo RNAi, we found that cosuppression of occludin and claudin-5 could establish a size-selective tight junction, enabling enhanced movement of Aβ from brain to blood in a murine model of AD. These findings suggest a counterintuitive and potentially beneficial correlation between the observed down-regulation of claudin-5 and occludin in AD brains and increased Aβ movement from the brain to the blood. Our observations suggest a mechanism whereby Aβ-mediated decreases in claudin-5 and occludin may allow for

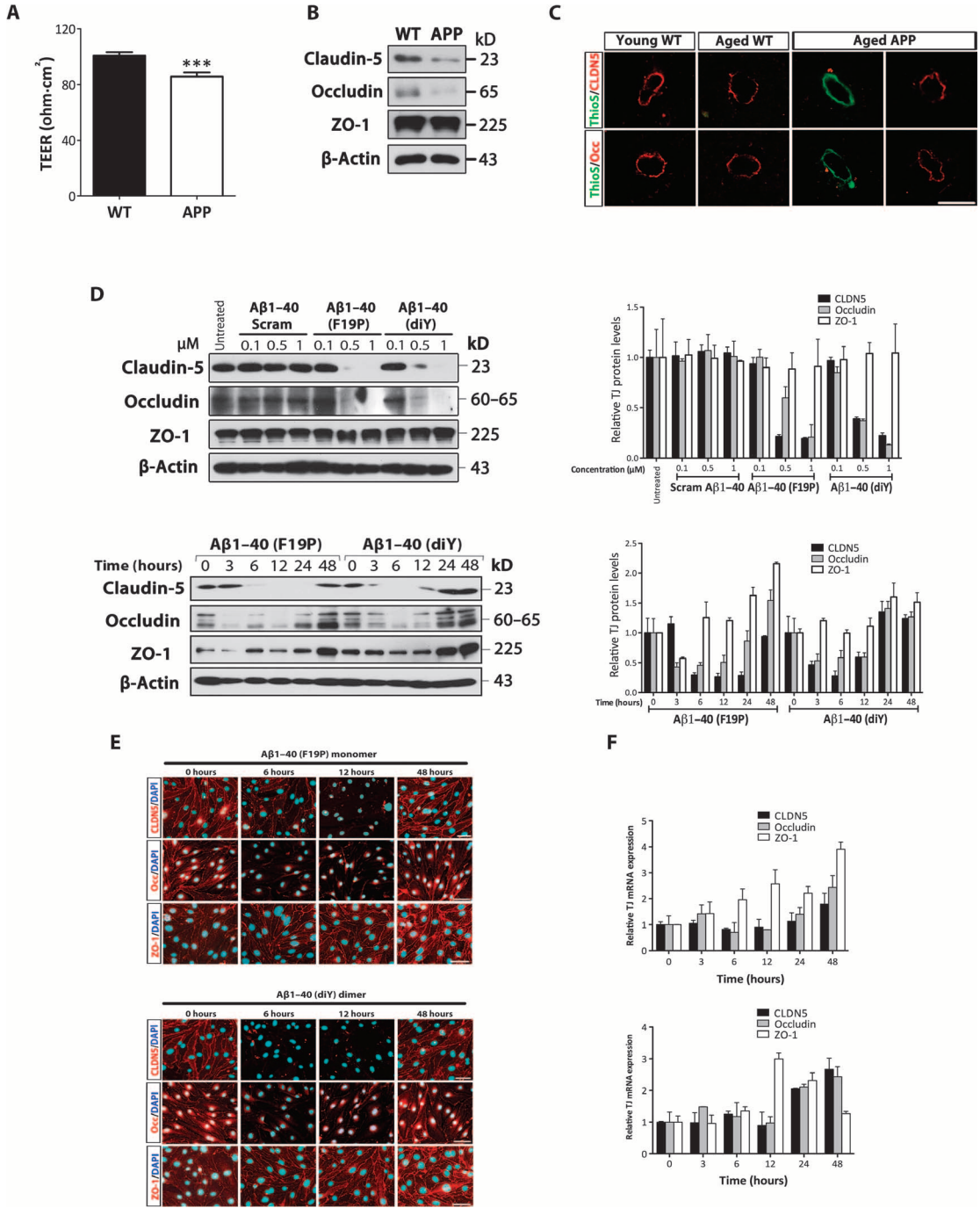

Fig. 5. Claudin-5 and occludin are reduced in CAA-affected microvessels of aged Tg2576 mouse brains and in response to Aβ(1–40) monomers and dimers in mouse brain endothelial cells. (**A**) TEER measurements across confluent monolayers of brain endothelial cells isolated from aged Tg2576 mice and age-matched wild-type (WT) controls (unpaired Student's *t* test: ***$P = 0.0005$; data are means ± SD, $n = 16$ Transwells per group). (**B**) Western blot analysis of tight junction proteins (claudin-5, occludin, ZO-1, and tricellulin) and Aβ transcellular receptors (LRP1 and RAGE) in brain endothelial cells isolated from aged (20 months) Tg2576 mice and age-matched WT controls ($n = 5$ animals per group). (**C**) Immunohistochemical analysis of claudin-5 and occludin in microvessels of young (3 months) and aged (20 months) WT mice and aged (20 months) Tg2576 mice (scale bar, 50 μm). (**D**) Top: Western blot (left) and densitometric analysis (right) of tight junction protein levels 12 hours after treatment of brain endothelial cells with increasing concentrations of scrambled Aβ(1–40) peptide, Aβ(1–40)F19P monomer, or Aβ(1–40)DiY dimer. Bottom: Western blot (left) and densitometric analysis (right) of tight junction protein levels over the course of 48 hours after treatment of brain endothelial cells with 1 μM of Aβ(1–40)F19P monomer or Aβ(1–40)DiY dimer (data are means ± SEM). (**E**) Immunocytochemical analysis of claudin-5, occludin, and ZO-1 in response to treatment of brain endothelial cells with 1 μM of Aβ(1–40)F19P monomer (top) or Aβ(1–40)DiY dimer (bottom) (images are representative of three separate cell transfections per time point; scale bars, 40 μm). (**F**) RT-PCR analysis of tight junction mRNA levels over the course of 48 hours in response to 1 μM of Aβ(1–40)F19P monomer (top) or Aβ(1–40)DiY dimer (bottom) (data are means ± SEM).

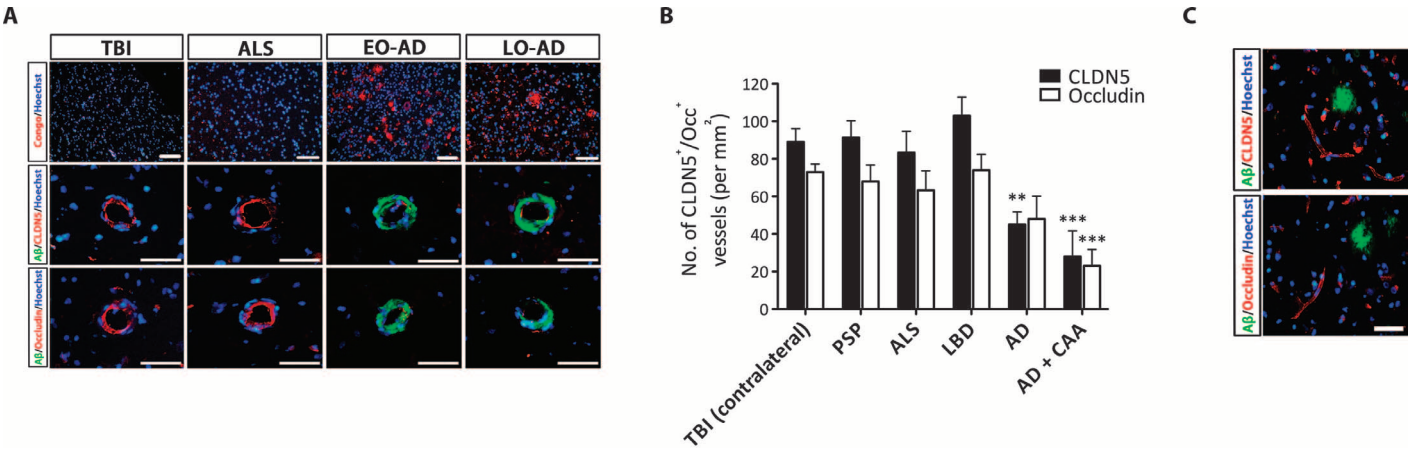

Fig. 6. Decreased levels of claudin-5 and occludin at the BBB segregate with Aβ/CAA in human AD brains. (**A**) Characterization of claudin-5 and occludin in brain microvessels and assessment of amyloid pathology (using Congo red and anti-Aβ immunostaining) in paraffin-embedded brain sections from a cohort of patients with neurological disease. Representative images from a nonneurodegenerative case [traumatic brain injury (TBI); contralateral region from injury site], a non-AD neurodegenerative case [amyotrophic lateral sclerosis (ALS)], and early-onset (EO) familial AD (*APP*-Iowa mutation) and late-onset (LO) sporadic AD cases (scale bar in all images, 50 μm). (**B**) Quantification of claudin-5– and occludin-positive vessels (per square millimeter) in donor brains from a cohort of patients with neurological disease (PSP, progressive supranuclear palsy; LBD, Lewy body dementia; one-way ANOVA followed by Bonferroni's post hoc test for multiple comparisons: $^{**}P \leq 0.01$ for claudin-5 in AD versus PSP, ALS, and LBD; $^{***}P \leq 0.001$ for claudin-5 in AD/CAA versus PSP, ALS, and LBD; $^{***}P \leq 0.001$ for occludin in AD/CAA versus PSP, ALS, and LBD; data are means ± SD). (**C**) Strong microvascular claudin-5 and occludin immunoreactivity in microvessels close to amyloid plaques in AD brains (scale bar, 50 μm).

size-selective paracellular movement of Aβ monomers, whereas high molecular weight oligomers formed after self-association of Aβ in AD brains may be too large to traverse the BBB and thus accumulate in the interstitial space (see the schematic in fig. S16).

It is possible that soluble Aβ(1–40) may facilitate its own movement across the tight junctions of the BBB in AD and thereby explain, in part, the amyloid sink hypothesis, according to which intravenously delivered antibodies (which do not cross the BBB) directed against Aβ can draw the molecule across the BBB in a therapeutic scenario (*29*, *30*). In a broader sense, our series of observations on the role of passive paracellular diffusion of Aβ(1–40) at the BBB highlights a novel method of Aβ movement from the brain to the blood and suggests that claudin-5 and occludin could represent novel therapeutic targets to modulate disease progression. Given that in vivo-jetPEI, the carrier agent used in this study, has already entered a range of clinical trials for systemic use with siRNAs, there is now a large portfolio of safety data pertaining to its use in humans. In addition, the vast body of clinical studies on the use of Aβ antibodies to treat AD patients (*30*) suggests that a controlled and targeted modulation of the BBB tight junctions as an adjunct to the amyloid sink hypothesis could now also represent a novel therapeutic paradigm in the treatment of AD.

MATERIALS AND METHODS

Animal experiments and experimental groups

Tg2576 mice (C57/Bl6;SJL background, stock no. 001349) carrying the human APP (APP_{695}) gene containing the double Swedish mutations (K670N and M671L) under the control of the hamster prion promoter were obtained from Taconic Europe. APPswe/PSEN1dE9 (also known as APP/PS1, stock no. 034829) carrying a chimeric mouse/human APP_{695} and a mutant human presenilin 1 (*PSEN1dE9*) were obtained from The Jackson Laboratory. Wild-type C57/Bl6J mice were sourced from The Jackson Laboratory and bred on-site in the Smurfit Institute of Genetics in Trinity College Dublin (TCD).

siRNA sequences and in vivo siRNA administration

Claudin-5 and occludin siRNAs were obtained from Dharmacon, and the sequences used were as follows: claudin-5 siRNA sense, 5′-CGUUGGAAAUUCUGGGUCUUU-3′, and antisense, 5′-AGACCCAGAAUUUCCAACGUU-3′; occludin siRNA sense, 5′-GAUAUUACUUGAUCGUGAUUU-3′, and antisense, 5′-AUCACGAUCAAGUAAUAUCUU-3′. Nontargeting negative control siRNA and mouse LRP1 siRNA (both Silencer) were obtained from Ambion. Preparation and administration of siRNA in vivo were performed as described previously (*26*). Briefly, 20 μg of siRNA was combined with 6.4 μl of in vivo-jetPEI (Polyplus Transfection) in a 10% glucose solution. The solution was mixed and incubated for 15 min at room temperature to allow the siRNA–in vivo-jetPEI complexes to form. A final volume of 400 μl was slowly injected into the mouse tail vein.

Aβ peptides

Aβ(1–40) and Aβ(1–40)F19P were synthesized and purified by J. I. Elliott at Yale University (New Haven, CT). Peptide masses and purities were determined by electrospray ionization/ion trap mass spectrometry and reversed-phase high-performance liquid chromatography, respectively. Dityrosine cross-linked Aβ dimer [Aβ(1–40)DiY] was prepared by oxidative cross-linking of Aβ(1–40) (*18*). Aβ(1–40) and Aβ(1–40)DiY were denatured by overnight incubation in 50 mM tris-HCl (pH 8.5) containing 7 M guanidinium-HCl and 5 mM EDTA. Monomer and dimer species were isolated by size exclusion chromatography with a Superdex 75 10/300 size exclusion column (GE Healthcare Biosciences) connected to a DuoFlow fast protein liquid chromatography system (Bio-Rad) and eluted in 50 mM ammonium bicarbonate (pH 8.5) (*18*). Peptide concentration was determined by ultraviolet absorbance at 275 nm. Aβ(1–40) aliquots (20 μM) were stored at −80°C until use, and Aβ(1–40)DiY aliquots were frozen and lyophilized. Scrambled

Aβ(1–40) peptide was obtained from Anaspec. FITC–Aβ(1–40) and FITC–Aβ(1–42) peptides were obtained from Bachem.

Endothelial cell culture and transfection

Mouse brain endothelial cells (Bend.3, American Type Culture Collection) were cultured in Dulbecco's modified Eagle's medium (DMEM) supplemented with 20% fetal calf serum and 2 mM sodium pyruvate in a 5% CO_2 incubator at 37°C. Bend.3 cells were seeded on 1% fibronectin–coated 24-well plates (1×10^5 cells per well), and 20 pmol siRNA was transfected per well using Lipofectamine 2000 (Invitrogen). RNA was extracted from Bend.3 cells, using the reagents and instructions supplied in the Qiagen RNeasy Mini Kit. Proteins were isolated with lysis buffer (62.5 mM tris, 2% SDS, 10 mM dithiothreitol, 10 μl protease inhibitor cocktail/100 ml) followed by centrifugation at 12,000 rpm for 20 min at 4°C, and supernatant was removed for tight junction protein analysis. All transfections were performed in both technical and biological triplicates.

Primary mouse brain endothelial cell isolation

Microvessels were isolated from the cortical gray matter of aged Tg2576 mice and age-matched wild-type controls by collagenase/dispase (Roche) digestion and bovine serum albumin density gradient centrifugation. Purified vessels were seeded at high density onto collagen IV/fibronectin–coated Corning HTS 24-well Transwell polyester inserts (0.4-μm pore size, vessels from five mouse brains per 3 ml). Cells were grown in EGM2-MV (Lonza) [with puromycin (5 μg/ml) during the first 5 days for endothelial cell selection] for 2 to 3 weeks until their TEER values plateaued.

Transwell permeability assays

Mouse brain endothelial cells (5×10^4 cells per well) were grown to confluence on 1% fibronectin–coated Corning HTS 24-well Transwell polyester inserts with a pore size of 0.4 μm and transfected with 10 pmol of targeting or nontargeting siRNAs, using Lipofectamine 2000 as described. Seventy-two hours after transfection, 10 μM of FITC–Aβ(1–40), FITC–Aβ(1–42), or FITC-inulin (Sigma-Aldrich) in DMEM was added to the apical chamber of each well, and the cells were incubated at 37°C. Sampling aliquots were taken from the basolateral chamber and replaced with fresh medium every 15 min for 2 hours and then transferred to 96-well plates (Nunc). FITC-Aβ fluorescence was determined using a spectrofluorometer (Optima Scientific) at an excitation wavelength of 485 nm and an emission wavelength of 520 nm. Relative fluorescence units were converted to values of nanograms per milliliter, using FITC-Aβ standard curves, and were corrected for background fluorescence and serial dilutions over the course of the experiment. For permeability assays measuring the basolateral to apical movement of FITC-Aβ, the peptide was added to the basolateral chamber, and sampling aliquots were taken from the apical side. For Transwell experiments involving synthetic Aβ(1–40)F19P monomer and Aβ(1–40)DiY dimer, 10 μM of either Aβ(1–40) monomer or dimer was applied to the apical chamber, and its movement across brain endothelial cell monolayers was measured using the Human Aβ40 ELISA kit (Invitrogen). The apparent permeability coefficient (P_{app}) for each treatment was calculated using the following equation:

$$P_{app}(\mathrm{cm/s}) = (\mathrm{d}Q/\mathrm{d}T)/(A \times C_0)$$

where $\mathrm{d}Q/\mathrm{d}T$ (μg/s) is the rate of appearance of Aβ peptide on the receiver side after application, A (cm^2) is the effective surface area of the insert size, and C_0 (μg/ml) is the initial Aβ peptide concentration on the donor side. $\mathrm{d}Q/\mathrm{d}T$ is the slope m ($y = mx + c$) calculated by plotting the cumulative amount (Q) versus time (s).

TEER measurements

Mouse brain endothelial cells were seeded on 1% fibronectin–coated Corning HTS 24-well Transwell polyester inserts as described. TEER was determined using an EVOM resistance meter with Endohm Chamber (World Precision Instruments) and a Millicell-Electrical Resistance System. Before measurements, both the apical and basolateral chambers were bathed in fresh medium at 37°C. The probe anode and cathode were carefully immersed in the chambers, and a current was passed across the cell monolayer. Changes in electrical resistance were measured in triplicate in units of ohm·cm^2, and the inherent resistance of a blank well coated with 1% fibronectin was subtracted from the values obtained.

Cell viability assays

Bend.3 cells were seeded on 1% fibronectin–coated 96-well plates at a density of 1.6×10^3 cells per well in DMEM. After 24 hours, Aβ(1–40)F19P monomer or Aβ(1–40)DiY dimer (0.5 to 5 μM) was applied to brain endothelial cells. At the time point of significant tight junction suppression (12 hours), the medium was replaced, and 20 μl of CellTiter 96 AQueous Non-Radioactive Cell Proliferation Assay reagent (Promega) was added to each well. The reagent was incubated with the cells for 2 hours, and the concentration of the formazan product was measured in a spectrophotometer at 490 nm.

Real-time reverse transcription polymerase chain reaction

Transcript levels were quantified using a one-step real-time reverse transcription polymerase chain reaction (RT-PCR) on the 7300 Real-Time PCR System (Applied Biosystems) with QuantiTect SYBR Green I (Qiagen) as a fluorescent dye. The QuantiTect One-Step RT-PCR Kit was able to support reverse transcription and subsequent gene-specific amplification in a single well. The RT-PCR reaction conditions were as follows: 50°C × 20 min, 95°C × 15 min, (95°C × 15 s, 60°C × 1 min) × 37, 95°C × 15 s, 60°C × 1 min, 95°C × 15 s, 60°C × 15 s. The primer sequences (designed using Primer3) for the RT-PCR experiments were supplied by Sigma-Aldrich and were as follows: claudin-5 left, 5′-TTTCTTCTATGCGCAGTTGG-3′, and right, 5′-GCAGTTTGGTGCCTACTTCA-3′; occludin left, 5′-ACAGTCCAATGGCCTACTCC-3′, and right, 5′-ACTTCAGGCACCAGAGGTGT-3′; ZO-1 left, 5′-CCACCTCTGTCCAGCTCTTC-3′, and right, 5′-CACCGGAGTGATGGTTTTCT-3′; β-actin left, 5′-TCACCCACACTGTGCCCATCTACGA-3′, and right, 5′-CAGCGGAACCGCTCATTGCCAATGG-3′. RT-PCR analysis was carried out on the 7300 Real-Time PCR System, and relative gene expression levels were measured using the comparative C_T method ($\Delta\Delta C_T$). Expression levels of target genes were standardized to the housekeeping gene β-actin. To assess the levels of RNAi-mediated tight junction suppression, results were also expressed as a percentage of the nontargeting siRNA control (normalized to β-actin) where applicable.

The levels of RNA isolated from mouse brain capillary fractions were also quantified in a StepOne Plus machine (Applied Biosystems) using TaqMan Gene Expression Assays (Applied Biosystems) with the following IDs: claudin-5, Mm00727012_s1; occludin, Mm00500912_m1. Target genes used a FAM reporter. The reaction conditions were as follows: 50°C × 2 min, 95°C × 20 s, (95°C × 1 s, 60°C × 20 s) × 40. Transcript levels were standardized using β-actin with a VIC reporter in the same well and assessed using the $\Delta\Delta C_T$ method.

Brain microvasculature fractionation

Hemibrains were homogenized in 5 ml of DMEM using a dounce homogenizer, and the homogenate was spun at 3000 rpm for 5 min. The resulting homogenate was incubated with 0.005% dispase (Sigma-Aldrich) for 2 hours at 37°C to dissociate the tissue. Homogenates were centrifuged at 3000 rpm for 5 min, and pellets were resuspended in a 12% dextran solution (M_w 70,000 from *Leuconostoc* spp.; Sigma) followed by centrifugation at 3000 rpm for 10 min at 4°C. The resulting capillary fraction was resuspended and washed with phosphate-buffered saline (PBS) and centrifuged at 2000 rpm for 5 min. Cells were resuspended in either RLT lysis buffer for RNA extractions using the Qiagen RNeasy Mini Kit or in protein lysis buffer for protein extraction.

Western blot analysis

The antibodies used were as follows: polyclonal rabbit anti–claudin-5 (1:500), polyclonal rabbit anti-occludin (1:1000), polyclonal rabbit anti–ZO-1, polyclonal rabbit anti-tricellulin (1:500; all from Invitrogen), polyclonal rabbit anti-LRP1 (C-terminal, 1:500; Sigma-Aldrich), polyclonal rabbit anti-RAGE (1:500), polyclonal rabbit anti-ApoE (1:500), and polyclonal rabbit anti–β-actin (1:2000; all from Abcam). AW7 antiserum recognizes multiple Aβ epitopes and aggregation states (*31*) and was used to detect Aβ. Briefly, membranes were incubated with primary antibody overnight at 4°C, washed with tris-buffered saline (TBS), and incubated with horseradish peroxidase (HRP)–conjugated goat anti-rabbit immunoglobulin G (IgG) secondary antibody (1:2000; Abcam) for 2 hours at room temperature. To detect HRP, immunoblots were incubated with enhanced chemiluminescence solution.

Immunocytochemistry and immunohistochemistry

Mouse brain endothelial cells were seeded on 1% fibronectin–coated Nunc Lab-Tek II Chamber Slides (Thermo Scientific) in DMEM. After siRNA treatment or treatment with Aβ(1–40) monomer or Aβ(1–40) dimer peptides, cells were fixed with 4% paraformaldehyde (PFA; pH 7.4); blocked with 5% normal goat serum (NGS); and incubated with polyclonal rabbit anti–claudin-5 (1:100), polyclonal rabbit anti-occludin (1:100), polyclonal rabbit anti–ZO-1 (1:100), or phalloidin–Alexa Fluor 488 (1:300; all from Invitrogen) overnight at 4°C. Cells were then incubated with Cy3-conjugated goat anti-rabbit secondary antibody (1:500; Abcam) for 3 hours at room temperature and counterstained with 4′,6-diamidino-2-phenylindole (DAPI; 1:5000). Mouse brain cryosections (12 μm thick) were permeabilized with 0.5% Triton X-100; blocked with 5% NGS; and incubated overnight with tight junction primary antibody, polyclonal rabbit anti–amyloid-β AW7 antibody (1:1000), or isolectin IB4–Alexa Fluor 488 (1:300; Invitrogen), as described (*18*, *19*). Sections were then incubated with Cy2- or Cy3-conjugated goat anti-rabbit IgG secondary antibody (1:500; Abcam) for 3 hours at room temperature and counterstained with DAPI. Analysis of stained cells or brain cryosections was performed using a Zeiss Axioplan 2 fluorescent microscope or an Olympus FluoView FV1000 confocal microscope with integrated software.

In vivo BBB permeability assays

The extent of BBB permeability was assessed by terminal perfusion of tracer molecules including 3- and 10-kD biotin-dextran (lysine-fixable, Invitrogen). After systemic siRNA administration and down-regulation of tight junction proteins, a PBS solution containing the tracer molecule (1 mg/ml) was slowly perfused into the left ventricle of anesthetized mice for 3 min using a peristaltic pump. Briefly, the thoracic cavity was quickly opened by cutting the ventral skin, peritoneal membrane, diaphragm, and rib cage to reveal the heart, with care taken to avoid cutting the visceral organs or large vessels. After tracer molecule perfusion, tissues including the brain, liver, lung, and heart were dissected and placed in 4% PFA (pH 7.4) overnight at 4°C. Tissues were then cryoprotected using a 10, 20, and 30% sucrose gradient, and 12-μm frozen sections were cut and incubated overnight with Cy3-conjugated streptavidin (1:100; Sigma-Aldrich) at 4°C. Analysis of tissue cryosections was performed on the same day using constant exposure settings on a Zeiss Axioplan 2 fluorescent microscope, and streptavidin-Cy3 fluorescence in tissue sections was quantified and compared using ImageJ software. Fluorescence values for tissue sections obtained from PBS-perfused animals without tracer were also measured as background controls. All perfusions and tissue analyses were performed blind to treatment.

Magnetic resonance imaging

After administration of targeting or nontargeting siRNAs, BBB integrity was assessed using a dedicated small-animal 7-T MRI system (Bruker BioSpec) at TCD. Mice were anesthetized with 5% isoflurane and placed on an MRI-compatible support cradle. This cradle has an in-built system for maintaining the animal's body temperature at 37°C, and a probe underneath the animal allows it to be physiologically monitored (electrocardiogram, respiration, and temperature). To ensure accurate positioning of the animal, an initial rapid pilot image was recorded and used to ensure correct geometry for all subsequent scans. The scale of BBB integrity was then visualized in high-resolution T1-weighted MR images [resolution, $0.156 \times 0.156 \times 5$ mm^3; field of view, $20 \times 20 \times 17.9$ mm^3; matrix, $128 \times 128 \times 30$; TR (repetition time)/TE (echo time), 500/2.7 ms; flip angle, 30°; number of averages, 3; acquisition time, 2 min, 24 s; repetitions, 8] before and after tail-vein administration of 100 μl of a 1:3 dilution of Gd-DTPA (0.5 M stock solution, Bayer), which was monitored over a period of 20 min after injection. MRI analysis was performed using ImageJ and MIPAV software, and all data were analyzed blind to treatment.

Plasma/brain tissue isolation and ELISA

Blood was collected from the tail veins of Tg2576 and APP/PS1 mice with a 30-gauge needle and transferred to cold EDTA-coated tubes. Samples were centrifuged at 1500 rpm for 10 min at 4°C, and the plasma phase was stored at −80°C. The mouse brain hippocampus was homogenized in ice-cold TBS and centrifuged at 16,000*g* for 30 min at 4°C. Supernatants were collected for analysis of soluble Aβ(1–40) levels, and pellets were resuspended in ice-cold guanidine buffer (5 M guanidine hydrochloride/50 mM tris-Cl, pH 8.0) for analysis of insoluble Aβ(1–42) levels. Plasma and brain Aβ(1–40) levels were quantified using the Human Aβ40 ELISA kit (Invitrogen). Absorbances were read at 450 nm on a spectrophotometer (Rosys 2010, Anthos), and Aβ concentrations were determined from the Aβ peptide standard curves after correcting for background absorbance and dilution factors. ELISA preparation and analysis were performed blind to treatment.

Hippocampal-linked spontaneous alternation task

T-maze trials were performed using a T-shaped apparatus consisting of three arms, with two situated at 180° from each other, and the third, representing the stem arm of the T, situated at 90° with respect to the other two. The protocol for spontaneous T-maze alternation as previously described was followed (*20*). All trials were performed blind to treatment. Briefly, the animal being tested was first placed at the start position located at the end of the stem arm. The door of the start position

was then released to allow the animal to choose one of the goal arms. Once inside one of the goal arms, the door of that arm was closed and the animal was confined there for 30 s. The animal was then placed back at the start position facing away from the goal arms for 15 s, the stem door was reopened, and the animal was given 2 min to choose one of the goal arms again. If the second choice of arm was different from the first, then the animal was scored as "alternating." Mice were tested three times per day for a period of 7 days.

Human brain sections

Paraffin-embedded blocks of postmortem human brain tissue from 30 deceased human subjects were obtained with ethical approval from the Dublin Brain Bank at Beaumont Hospital in Dublin, Ireland. Brain regions and neuropathological diagnosis for each subject are provided in table S1. Sections (10 μm) were cut from paraffin-embedded blocks with a microtome (Leica), and after xylene deparaffinization/ethanol rehydration, antigen retrieval was performed by boiling the sections for 2 × 5 min rounds in sodium citrate buffer (10 mM sodium citrate, 0.05% Tween 20, pH 6.0). The sections were incubated with Congo red stain (Sigma-Aldrich) for 30 min as per the manufacturer's instructions and counterstained with Hoechst 33342 (1:10,000). For immunostaining of amyloid-β and claudin-5/occludin, sections were blocked with 5% NGS and double-stained by incubating with polyclonal rabbit anti–amyloid-β (AW7, 1:500) and monoclonal mouse anti–claudin-5 (1:100; Invitrogen) or monoclonal anti-occludin (1:100; Invitrogen) overnight at 4°C. Brain sections were then incubated with Cy2-conjugated goat anti-mouse IgG and Cy3-conjugated goat anti-rabbit (1:500; both from Abcam) for 3 hours at room temperature and counterstained with Hoechst 33342. Analysis of the brain sections was performed using a Zeiss Axioplan 2 fluorescent microscope. Cutting of sections, staining, and microscopy were performed blind to neuropathological diagnosis.

Statistics

For each data set, the mean (μ), SD, and SEM were calculated. A two-tailed unpaired Student's *t* test was used to evaluate the significance of differences between each data set and the corresponding nontargeting control. Differences were considered statistically significant when *P* values were ≤0.05. For multiple comparisons, as was the case for comparison of permeability coefficients (P_{app}) between siRNA treatments, ANOVA followed by a Bonferroni posttest for multiple comparisons was used, with $P \leq 0.05$ representing significance.

Study approval

All procedures involving experimental animals, carried out in the Smurfit Institute of Genetics in TCD, adhered to the principles laid out by the internal ethics committee at TCD, and all relevant national licenses were obtained before commencement of work.

SUPPLEMENTARY MATERIALS

Supplementary material for this article is available at http://advances.sciencemag.org/cgi/content/full/1/8/e1500472/DC1

Fig. S1. Western blot of ZO-1 levels 24 to 96 hours after siRNA transfection (top panel; NT, nontargeting siRNA; C/O, claudin-5 and occludin siRNAs) and densitometric analysis of relative ZO-1 protein levels normalized to NT siRNA sample at each time point (bottom panel; data are means ± SEM).

Fig. S2. FITC–Aβ(1–42) peptide was applied to the apical chamber of a Transwell plate 72 hours after siRNA treatment of Bend.3 cells, and its movement across cell monolayers was monitored by fluorescence spectrophotometry over the course of 2 hours (left panel).

Fig. S3. FITC-inulin was applied to the basolateral chamber of a Transwell plate 72 hours after siRNA treatment of Bend.3 cells, and its movement across cell monolayers was monitored by fluorescence spectrophotometry over the course of 2 hours.

Fig. S4. Down-regulation of claudin-5, occludin, and LRP1 in primary mouse brain endothelial cells and analysis of FITC–Aβ(1–40) movement.

Fig. S5. FITC–Aβ(1–40) (10 nM) was applied to the basolateral chamber of a Transwell plate 72 hours after siRNA treatment of Bend.3 cells, and its movement across cell monolayers was assessed by ELISA over the course of 2 hours (left panel).

Fig. S6. Relative purity of mouse brain capillary fractions isolated using a dispase/dextran method.

Fig. S7. Occludin expression and BBB permeability in APPP/PS1 mice post suppression of tight junctions.

Fig. S8. Analysis of peripheral organ permeability post suppression of claudin-5 and occludin.

Fig. S9. Increased plasma levels of Aβ in APP/PS1 mice post suppression of claudin-5 and occludin.

Fig. S10. Aβ in retinas of 8-month-old siRNA-treated DBA/2J mice.

Fig. S11. Analysis of BBB integrity to endogenous immunoglobulin G (IgG) after chronic intravenous administration of nontargeting (NT) siRNA or claudin-5 and occludin (C/O) siRNAs in Tg2576 mice (scale bar, 100 μm; *n* = 5 to 6 animals per experimental group; data are means ± SEM).

Fig. S12. Hematoxylin and eosin (H&E) staining of liver, lung, heart, spleen, and kidney paraffin-embedded sections from nontargeting (NT) siRNA–treated and claudin-5 and occludin (C/O) siRNA–treated APP (Tg2576) transgenic mice at 12 months of age (*n* = 4 to 6 animals per experimental group; scale bar for all images, 200 μm).

Fig. S13. Quantification of claudin-5– and occludin-positive vessels in young WT, aged WT, and aged Tg2576 animals (*n* = 4 animals per group; data are means ± SEM).

Fig. S14. Western blot analysis of tight junction protein levels in Bend.3 cells 12 hours after treatment with increasing concentrations (0.1 to 1 μM) of recombinant unmodified Aβ(1–40) monomer peptides (*n* = 3 separate cell transfections per concentration).

Fig. S15. MTS-based cell viability assay measured 12 hours after treatment of Bend.3 cells with increasing concentrations (0.5 to 5 μM) of Aβ(1–40)F19P monomer or Aβ(1–40)DiY dimer.

Fig. S16. Schematic model of paracellular Aβ movement across CVECs of the BBB.

Table S1. Brain regions, pathological diagnoses, age, gender, and postmortem (PM) interval for the neurological disease patient cohort examined in this study.

REFERENCES AND NOTES

1. M. Prince, R. Bryce, E. Albanese, A. Wimo, W. Ribeiro, C. P. Ferri, The global prevalence of dementia: A systematic review and metaanalysis. *Alzheimers Dement.* **9**, 63–75.e2 (2013).
2. D. W. Dicksen, The pathogenesis of senile plaques. *J. Neuropathol. Exp. Neurol.* **56**, 321–339 (1997).
3. A. E. Roher, K. C. Palmer, V. Chau, M. J. Ball, Isolation and chemical characterization of Alzheimer's disease paired helical filament cytoskeletons: Differentiation from amyloid plaque core protein. *J. Cell Biol.* **107**, 2703–2716 (1988).
4. G. M. Shankar, S. Li, T. H. Mehta, A. Garcia-Munoz, N. E. Shepardson, I. Smith, F. M. Brett, M. A. Farrell, M. J. Rowan, C. A. Lemere, C. M. Regan, D. M. Walsh, B. L. Sabatini, D. J. Selkoe, Amyloid-β protein dimers isolated directly from Alzheimer's brains impair synaptic plasticity and memory. *Nat. Med.* **14**, 837–842 (2008).
5. K. G. Mawuenyega, W. Sigurdson, V. Ovod, L. Munsell, T. Kasten, J. C. Morris, K. E. Yarasheski, R. J. Bateman, Decreased clearance of CNS β-amyloid in Alzheimer's disease. *Science* **330**, 1774 (2010).
6. A. P. Sagare, R. D. Bell, B. V. Zlokovic, Neurovascular defects and faulty amyloid-β vascular clearance in Alzheimer's disease. *J. Alzheimers Dis.* **33** (Suppl. 1), S87–S100 (2013).
7. E. Auriel, S. M. Greenberg, The pathophysiology and clinical presentation of cerebral amyloid angiopathy. *Curr. Atheroscler. Rep.* **14**, 343–350 (2012).
8. N. J. Abbott, A. A. K. Patabendige, D. E. M. Dolman, S. R. Yusof, D. J. Begley, Structure and function of the blood-brain barrier. *Neurobiol. Dis.* **37**, 13–25 (2010).
9. B. Obermeier, R. Daneman, R. M. Ransohoff, Development, maintenance and disruption of the blood-brain barrier. *Nat. Med.* **19**, 1584–1596 (2013).
10. R. Daneman, L. Zhou, D. Agalliu, J. D. Cahoy, A. Kaushal, B. A. Barres, The mouse blood-brain barrier transcriptome: A new resource for understanding the development and function of brain endothelial cells. *PLOS One* **5**, e13741 (2010).
11. N. R. Saunders, R. Daneman, K. M. Dziegielewska, S. A. Liddelow, Transporters of the blood–brain and blood–CSF interfaces in development and in the adult. *Mol. Aspects Med.* **34**, 742–752 (2013).
12. R. Deane, S. D. Yan, R. K. Submamaryan, B. LaRue, S. Jovanovic, E. Hogg, D. Welch, L. Manness, C. Lin, J. Yu, H. Zhu, J. Ghiso, B. Frangione, A. Stern, A. M. Schmidt, D. L. Armstrong, B. Arnold, B. Liliensiek, P. Nawroth, F. Hofman, M. Kindy, D. Stern, B. Zlokovic, RAGE mediates amyloid-β peptide transport across the blood-brain barrier and accumulation in brain. *Nat. Med.* **9**, 907–913 (2003).

13. R. Deane, Z. Wu, A. Sagare, J. Davis, S. D. Yan, K. Hamm, F. Xu, M. Parisi, B. LaRue, H. W. Hu, P. Spijkers, H. Guo, X. Song, P. J. Lenting, W. E. Van Nostrand, B. V. Zlokovic, LRP/amyloid β-peptide interaction mediates differential brain efflux of Aβ isoforms. *Neuron* **43**, 333–344 (2004).
14. A. Carrano, J. J. M. Hoozemans, S. M. van der Vies, A. J. M. Rozemuller, J. van Horssen, H. E. de Vries, Amyloid beta induces oxidative stress-mediated blood–brain barrier changes in capillary amyloid angiopathy. *Antioxid. Redox Signal.* **15**, 1167–1178 (2011).
15. K. E. Biron, D. L. Dickstein, R. Gopaul, W. A. Jeffries, Amyloid triggers extensive cerebral angiogenesis causing blood brain barrier permeability and hypervascularity in Alzheimer's disease. *PLOS One* **6**, e23789 (2011).
16. A. M. Hartz, B. Bauer, E. L. Soldner, A. Wolf, S. Boy, R. Backhaus, I. Mihaljevic, U. Bogdahn, H. H. Klünemann, G. Schuierer, F. Schlachetzki, Amyloid-β contributes to blood–brain barrier leakage in transgenic human amyloid precursor protein mice and in humans with cerebral amyloid angiopathy. *Stroke* **43**, 514–523 (2012).
17. D. M. Walsh, A. Lomakin, G. B. Benedek, M. M. Condron, D. B. Teplow, Amyloid β-protein fibrillogenesis: Detection of a protofibrillar intermediate. *J. Biol. Chem.* **272**, 22364–22372 (1997).
18. T. T. O'Malley, N. A. Oktaviani, D. Zhang, A. Lomakin, B. O'Nuallain, S. Linse, G. B. Benedek, M. J. Rowan, F. A. A. Mulder, D. M. Walsh, Aβ dimers differ from monomers in structural propensity, aggregation paths, and population of synaptotoxic assemblies. *Biochem. J.* **461**, 413–426 (2014).
19. M. Campbell, A.-S. Kiang, P. F. Kenna, C. Kerskens, C. Blau, L. O'Dwyer, A. Tivnan, J. A. Kelly, B. Brankin, G.-J. Farrar, P. Humphries, RNAi-mediated reversible opening of the blood-brain barrier. *J. Gene Med.* **10**, 930–947 (2008).
20. T. Kawarabayashi, L. H. Younkin, T. C. Saido, M. Shoji, K. H. Ashe, S. G. Younkin, Age-dependent changes in brain, CSF, and plasma amyloid β protein in the Tg2576 transgenic mouse model of Alzheimer's disease. *J. Neurosci.* **21**, 372–381 (2001).
21. R. M. J. Deacon, J. N. P. Rawlins, T-maze alternation in the rodent. *Nat. Protoc.* **1**, 7–12 (2006).
22. D. Goldblum, A. Kipfer-Kauer, G.-M. Sarra, S. Wolf, B. E. Frueh, Distribution of amyloid precursor protein and amyloid-β immunoreactivity in DBA/2J glaucomatous mouse retinas. *Invest. Ophthalmol. Vis. Sci.* **48**, 5085–5090 (2007).
23. T. Kanekiyo, H. Xu, G. Bu, ApoE and Aβ in Alzheimer's disease: Accidental encounters or partners? *Neuron* **81**, 740–754 (2014).
24. A. Goate, M.-C. Chartier-Harlin, M. Mullan, J. Brown, F. Crawford, L. Fidani, L. Giuffra, A. Haynes, N. Irving, L. James, R. Mant, P. Newton, K. Rooke, P. Roques, C. Talbot, M. Pericak-Vance, A. Roses, R. Williamson, M. Rossor, M. Owen, J. Hardy, Segregation of a missense mutation in the amyloid precursor protein gene with familial Alzheimer's disease. *Nature* **349**, 706–707 (1991).
25. S. Gandy, Lifelong management of amyloid-beta metabolism to prevent Alzheimer's disease. *N. Engl. J. Med.* **367**, 864–865 (2012).
26. T. Nitta, M. Hata, S. Gotoh, Y. Seo, H. Sasaki, N. Hashimoto, M. Furuse, S. Tsukita, Size-selective loosening of the blood-brain barrier in claudin-5–deficient mice. *J. Cell Biol.* **161**, 653–660 (2003).
27. M. Campbell, F. Hanrahan, O. L. Gobbo, M. E. Kelly, A.-S. Kiang, M. M. Humphries, A. T. H. Nguyen, E. Ozaki, J. Keaney, C. W. Blau, C. M. Kerskens, S. D. Cahalan, J. J. Callanan, E. Wallace, G. A. Grant, C. P. Doherty, P. Humphries, Targeted suppression of claudin-5 decreases cerebral oedema and improves cognitive outcome following traumatic brain injury. *Nat. Commun.* **3**, 849 (2012).
28. L. M. Tai, K. A. Holloway, D. K. Male, A. J. Loughlin, I. A. Romero, Amyloid-β-induced occludin down-regulation and increased permeability in human brain endothelial cells is mediated by MAPK activation. *J. Cell. Mol. Med.* **14**, 1101–1112 (2010).
29. E. Karran, M. Mercken, B. De Strooper, The amyloid cascade hypothesis for Alzheimer's disease: An appraisal for the development of therapeutics. *Nat. Rev. Drug Discov.* **10**, 698–712 (2011).
30. J. H. Toyn, M. K. Ahlijanian, Interpreting Alzheimer's disease clinical trials in light of the effects on amyloid-β. *Alzheimers Res. Ther.* **6**, 14 (2014).
31. J. M. McDonald, N. J. Cairns, L. Taylor-Reinwald, D. Holtzman, D. M. Walsh, The levels of water-soluble and triton-soluble Aβ are increased in Alzheimer's disease brain. *Brain Res.* **1450**, 138–147 (2012).

Acknowledgments: We would like to thank C. Woods, C. Murray, and D. Flynn for animal husbandry. **Funding:** This work was supported by grants from Science Foundation Ireland (SFI) (12/YI/B2614; 08/IN.I/B2033), The Bright Focus Foundation, and Enterprise Ireland. The Ocular Genetics Unit at TCD is supported by SFI, the Health Research Board of Ireland, the U.S. Department of Defense [Telemedicine and Advanced Technology Research Center (TATRC)], and the European Research Council. This work was also supported in part by NIH grant AG046275 to D.M.W. J.K. was supported by a Postgraduate Research Scholarship from the Irish Research Council. **Author contributions:** J.K.: Performed experiments and wrote the paper. D.M.W.: Experimental design and reagents. T.O.: Preparation of Aβ peptides. N.H.: Isolation of primary mouse brain endothelial cells and TEER analysis. D.E.C.: DBA mouse tissue processing and Western blot analysis. T.L. and F.S.: Selection and processing of postmortem human tissue specimens. J.M.: Western blot analysis. M.M.H.: Design and analysis of experiments and data. J.J.C.: Pathological analysis of murine tissues. M.A.F. and F.M.B.: Pathological and histopathological analysis and diagnosis of postmortem human brain tissue. P.H.: Design and analysis of experiments and data. M.C.: Conceived, designed, and performed experiments and wrote the paper. **Competing interests:** Trinity College Dublin owns a patent portfolio related to the use of RNAi to modulate the BBB. **Data and materials availability:** All data associated with this study is in the body of the manuscript.

Submitted 20 April 2015
Accepted 1 July 2015
Published 18 September 2015
10.1126/sciadv.1500472

Citation: J. Keaney, D. M. Walsh, T. O'Malley, N. Hudson, D. E. Crosbie, T. Loftus, F. Sheehan, J. McDaid, M. M. Humphries, J. J. Callanan, F. M. Brett, M. A. Farrell, P. Humphries, M. Campbell, Autoregulated paracellular clearance of amyloid-β across the blood-brain barrier. *Sci. Adv.* **1**, e1500472 (2015).

ScienceAdvances
AAAS

Autoregulated paracellular clearance of amyloid-β across the blood-brain barrier

James Keaney, Dominic M. Walsh, Tiernan O'Malley, Natalie Hudson, Darragh E. Crosbie, Teresa Loftus, Florike Sheehan, Jacqueline McDaid, Marian M. Humphries, John J. Callanan, Francesca M. Brett, Michael A. Farrell, Peter Humphries and Matthew Campbell (September 18, 2015)

Sci Adv 2015, 1:.
doi: 10.1126/sciadv.1500472